

## AN INVESTIGATION OF FILM WAVY STRUCTURE IN ANNULAR FLOW USING TWO SIMULTANEOUS LIF APPROACHES

A.V. Cherdantsev<sup>1,2\*</sup>, J.S. An<sup>1</sup>, I. Zadrazil<sup>1</sup>, C.N. Markides<sup>1</sup>

\*Author for correspondence

<sup>1</sup>Clean Energy Processes (CEP) Laboratory, Department of Chemical Engineering, Imperial College London, London, UK

<sup>2</sup>Kutateladze Institute of Thermophysics, Novosibirsk, Russia

E-mail: [cherdantsev@itp.nsc.ru](mailto:cherdantsev@itp.nsc.ru)

### ABSTRACT

The paper is devoted to development and validation of film thickness measurement techniques in interfacial gas-liquid flows. The specific flow investigated here is that of downwards (co-flowing) annular flow in a vertical pipe, however, many of the observations and findings are transferable to similar flow geometries. Two advanced spatially resolved techniques, namely planar laser-induced fluorescence and brightness-based laser-induced fluorescence, are used simultaneously in the same area of interrogation. A single laser sheet is used to excite fluorescence along one longitudinal section of the pipe, and two cameras (one for each method) are placed at different angles to the plane of the laser sheet in order to independently recover the shape of the interface along this section. This allows us to perform a cross-validation of the two techniques and to analyse their respective characteristics, advantages and shortcomings.

### INTRODUCTION

In the two-phase vertical flow regime of co-flowing gas-liquid annular flow, the liquid phase flows as a film along channel wall in the direction of gravity, and in the same direction as the gaseous core of the duct. At large enough gas and liquid flow rates liquid droplets are entrained from the film surface into the gas core and gas bubbles are entrapped by the liquid film. The film surface in annular flow is covered by a multi-scale system of waves, in which disturbance waves dominate due to their high amplitude, velocity, longitudinal size and lifetime. Disturbance waves are considered the main and necessary source of liquid entrainment; they carry the major portion of liquid and they also exert strong influence on pressure drop and heat transfer in the flow. The disturbance waves are covered with small-scale ripple waves that are generated at their rear slopes [1]. These ripples accelerate and travel across the top of the disturbance waves until they are scattered as droplets by the gas stream. The entrained droplets eventually deposit back onto the film surface leading to possible entrapment of gas bubbles into the liquid film [2].

The experimental investigation of the wavy structure of liquid films in annular flow is a strong challenge since it has strong requirements from the measuring system. In particular, it demands that measurements should be resolved in space and time simultaneously, with high temporal and spatial resolution. The size of the area of interrogation should be large enough in both the spatial and temporal domains. In addition, ideally, the measurements should be resolved along both longitudinal and circumferential coordinates, since ripples have complicated three-dimensional structure, while simultaneous velocity

information in both the gas and liquid phase is of strong interest in understanding some of the interfacial wave phenomena.

A number of experimental methods are available for the study of liquid films in annular flow but only few of these satisfy many of the requirements listed above. In particular we are interested here in two methods based on the same physical principle of laser-induced fluorescence (LIF), which differ in the method of data recovery. The first approach is widely known as planar LIF, or PLIF. In this approach, the laser sheet illuminates one longitudinal section of the duct, which causes the liquid to emit red-shifted fluorescent light. A camera with an optical filter can be used to directly image the shape of the emitting longitudinal section of the film, which gives instantaneous local film thickness. Such an approach was used in Refs. [3-6]. This method has very high spatial resolution; the data can be spatiotemporally resolved and they are not expected to be affected by steep and curved interfaces or the bubbles. One more advantage is that it can be used simultaneously with particle velocimetry techniques to study the velocity field inside the liquid film revealing links to local film thickness, as done in Ref. [7]. One limitation of this method consists in an inability to perform three-dimensional measurements, though transverse profiles of film thickness can be obtained separately [5]. The other limitation may be related to the "mirror effect", caused by total internal reflection (TIR) of the fluorescent light at the curved interface between the laser sheet and the camera [8].

The second approach of interest based on the LIF principle is sometimes called brightness-based LIF or BBLIF. In this approach the integrated local brightness of fluorescent light is measured with a camera and is converted into a local film thickness using the Lambert-Beer law. This method was used to study liquid film structure in annular flow in both 2D [1,9] and 3D [10] configurations, together with droplets entrainment and deposition and bubbles entrapment [2,10]. This technique has high space and time resolution characteristics, and does not suffer from same TIR mirror-effect issues of PLIF. On the other hand, it cannot provide velocity information in a single measurement, and careful attention must be placed on the processing of the raw signal to overcome issues relating to fluorescence signal variations due to high curvature or bubble/droplet presence along the laser sheet (including due to TIR).

In the present work, the wavy structure of liquid films in downwards annular flow is studied by both techniques simultaneously. This allows us to perform a detailed cross-validation of the two techniques on different features appearing in the flow, such as bubbles, steep slopes, etc. It also offers us the interesting possibility to investigate directly the mirror

effect predicted analytically by Ref.[8], to check the validity of the PLIF approach. The main goal of the paper is to investigate the strengths and weaknesses of each of the two techniques and to devise solutions to eliminate or minimise the limitations.

## EXPERIMENTAL METHODS

The experiments were performed in a downward annular flow facility at Imperial College London, known as DAFLOF, comprising a vertical pipe with an inner diameter of 32.4 mm and a total measurement length of 4 m. The pipe was made of fluorinated ethylene propylene (FEP) to match the refractive index of water. Tap water with a small addition of Rhodamine 6G dye (8 mg/L) was used as the working liquid. A schematic of the experimental arrangement is shown in Fig. 1.

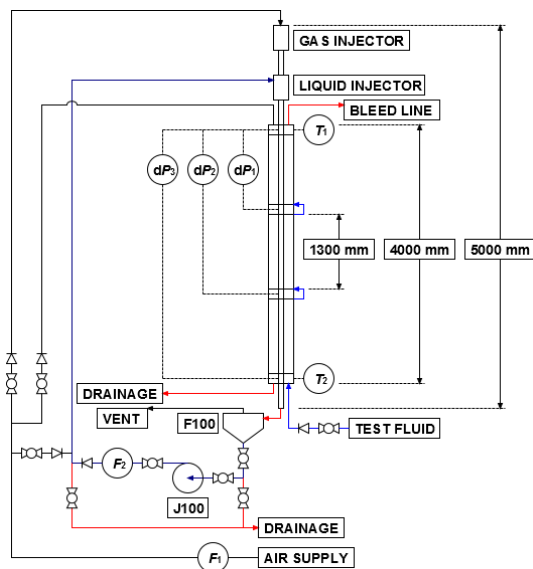


**Figure 1** Schematic diagram of the DAFLOF facility

The liquid phase was circulated around the system by a variable speed pump and introduced into the test section via a conical injector. The pipe was enclosed in a Perspex box filled with water to minimise optical distortions caused by the cylindrical geometry of the pipe. Experiments were performed over a range of superficial gas velocities,  $V_g$ , from 0 to 39 m/s, and liquid Reynolds numbers,  $Re_L$ , from 150 to 1350. Here,  $Re_L = Q/\pi D\nu$ , where  $Q$  is volumetric liquid flow rate,  $D$  is pipe inner diameter and  $\nu$  is kinematic viscosity of liquid.

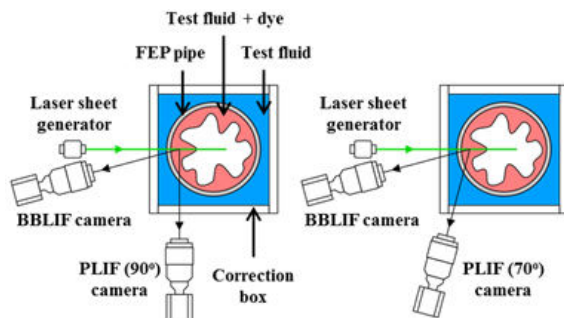


**Figure 2** Top view of the layout of the cameras and laser sheet for the PLIF90 (left) and PLIF70 (right) configurations.

A pulsed Nd:YAG laser was used for the excitation of the fluorescent dye. The laser beam was converted into a vertical optical sheet, focused at the nearest inner wall of the pipe. The width of the laser sheet was about 0.4 mm. Two CMOS cameras were located at the same distance from the inlet and aimed at approximately the same area. Both cameras were equipped with Sigma 105 mm f/2.8 macro lenses and long-pass filters. The BBLIF camera was placed next to the laser at an angle of  $10^\circ$  to the plane of the laser sheet. The PLIF camera was placed at an angle of either  $90^\circ$  or  $70^\circ$  to the plane of the laser sheet (see Fig. 2). The angle of the PLIF camera was varied in order to investigate its influence on the results of PLIF measurement.

To identify the spatial (pixel) resolution and relate the areas viewed by the two cameras, a calibration target was inserted inside the pipe and aligned with the plane of the laser sheet; the pipe was filled with the working liquid. A combined image of the graticule obtained by both cameras for PLIF90 is shown in Fig. 3, with the PLIF image at the top. A transformation was then obtained by linear correspondence of the coordinates of several squares in both images. The length of the overlapping area was found to be 34.3 mm for PLIF90 and 31.5 mm for PLIF70. The spatial resolution for PLIF90 was  $30.6 \mu\text{m}/\text{pixel}$ ; for PLIF70 it was  $26.6 \mu\text{m}/\text{pixel}$  in the longitudinal direction and  $28 \mu\text{m}/\text{pixel}$  in radial one. The spatial resolution of the BBLIF image in the longitudinal direction was  $26.7 \mu\text{m}/\text{pixel}$ .

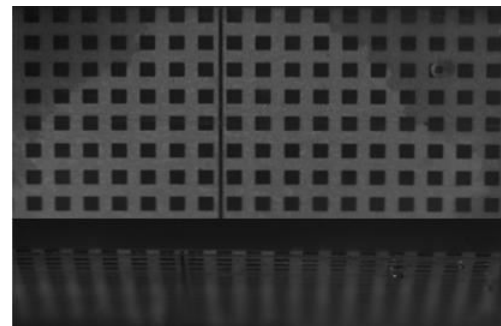


**Figure 3** Combined image of the calibration graticule inside the water-filled pipe: PLIF90 (top) and BBLIF (bottom).

The pulse rate of laser used in this work (and, hence, the frame rate of the cameras) was 100 Hz, and the exposure time defined by duration of the laser pulse was 10 ns. The frame rate used is not sufficient for a comprehensive investigation of the full temporal evolution of the waves of different types in all flow conditions. Nonetheless, the instantaneous shape of the interface obtained by the two cameras simultaneously is enough for the goal of the present work. For each flow condition (set of gas and liquid flow rates), a sequence of 1000 frames was recorded, corresponding to a duration of 10 s. The conventional method of processing of PLIF images consists in identifying the position of the boundaries of the illuminated area based on a brightness threshold [4-6]. The BBLIF data processing was made for the central line of the illuminated area to form spatiotemporal matrices of raw brightness for each flow regime from the whole sequence of frames. The conversion of local brightness into a film thickness measurement was based on

integration of the Lambert-Beer law [9]. A record at  $Re_L=150$  and  $V_g=0$  was used as a reference signal for this process.

## RESULTS

The two main wave patterns for downward annular flow are referred to as the ‘dual-wave’ regime and ‘regular disturbance wave’ regime [11]. The main criterion used to identify the transition between the two is how smooth or agitated the film surface is; strong agitation corresponds to massive entrapment of gaseous bubbles into the liquid film. Transition in the present experiments roughly corresponds to that in Ref. [11].

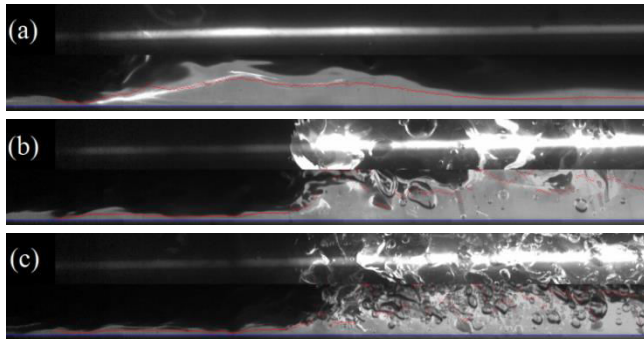


**Figure 4** Raw BBLIF/PLIF70 images of large waves for  $Re_L=300$ , and: (a)  $V_g=16$  m/s; (b)  $V_g=20$  m/s; (c)  $V_g=24$  m/s.

The difference is most clearly manifested when the largest waves are studied. An example of how the transition occurs is shown in Fig. 4 for  $Re_L=300$  for three values of  $V_g$ . In each image the top portion represents a raw BBLIF image rescaled longitudinally to correspond to the PLIF image, and the bottom part shows raw PLIF70 image together with processed film thickness result calculated by BBLIF, shown by red dots. At  $V_g=16$  m/s there are no bubbles and the interface is smooth (the bright line in the PLIF image will be discussed later). At  $V_g=20$  m/s occasional large bubbles appear in the film and the interface shows the presence of roughness which causes optical distortions in the BBLIF data. At  $V_g=24$  m/s the number of bubbles sharply increases together with a decrease in the average size of the bubbles; the interfacial roughness becomes much more significant with smaller wavelengths.

### Mirror effect

Figure 5 shows a direct comparison of raw PLIF and BBLIF signals for a falling film at  $Re_L=300$  superimposed in the same manner as in was made in Fig. 4. There is an obvious discrepancy between the two results: the film thickness profile obtained when processing the BBLIF image shows lower thickness values than those obtained by measuring the width of the full illuminated area in raw PLIF images. The discrepancy is stronger for the 70° case. In the PLIF90 case, the front of the wave appears upstream in the BBLIF signal compared to the PLIF signal. Such a situation does not occur with each wave, but it is rather frequent.

A closer examination of the raw PLIF images shows that there is a distinct bright line inside the illuminated area; the position of this line coincides often with the local film thickness measured by the BBLIF method. Such a line was also observed in earlier PLIF data [6] (see Fig. 2a and 3b in this

paper). We suppose that this line corresponds to the real position of the interface, and that the illuminated area above it is likely related to the mirror effect, described theoretically in Ref. [8]. According to this model, the reemitted fluorescent light, produced by the illuminated section of liquid film, emits in all directions; part of it goes straight into the camera, creating the real image of the film profile. At the same time, light emitted under an angle undergoes total internal reflection at the interface between the laser plane and the camera (see Fig. 2 in Ref. [8], or Fig. 7a in the present paper), and creates a false reflected image of the film above the true image. As a result of ray-tracing modelling, the PLIF90 image of the film is expected to look as shown in Fig. 6a, with an overestimation of film thickness by 29% for the case of waveless films inside 24 mm i.d. pipe in the range of 0.3-1.5 mm thickness.

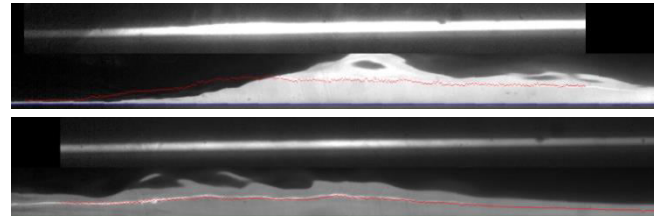


**Figure 5** Comparison of raw PLIF and BBLIF results in the falling film regime ( $Re_L=300$ ,  $V_g=0$ ). (a) PLIF90; (b) PLIF70.

Beyond the correlation between the processed BBLIF signal result and the bright line in raw PLIF images, two indirect supporting considerations seem to suggest that this explanation is valid. First, images of bubbles entrapped in the film both in and out of the laser sheet appear doubled by the reflected image located above the bright line. Second, a supporting observation is related to the appearance of slightly darker inclined streaks, which most likely are shadows of tiny objects on the wall (which may be speckles of dirt, tiny bubbles at the outer surface of the pipe or non-uniformities in the pipe material). The laser was located slightly above the area of interrogation, so these lines are inclined at a corresponding angle. It can be seen that these lines are broken when they cross the bright line. Importantly, however, the shape of the brightness profile in the experiments (Fig. 6b) is different from that assumed in Ref. [8] (Fig. 6a).

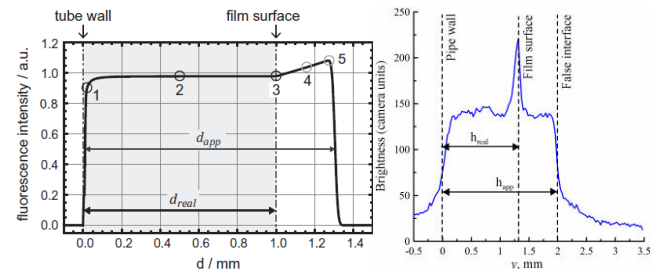


**Figure 6** (a) Assumed brightness distribution in a raw PLIF90 image along the radial coordinate (Fig. 3 in Ref. [8]). (b) Example of brightness profile from experimental PLIF image.

The difference is manifested in the presence of a peak in brightness at the supposed position of the true interface. It can

be seen that in the case of PLIF70 the peak is located farther from the false interface. To verify the influence of the PLIF angle, a simple geometrical calculation was performed for the case of a waveless film. The calculation analyses the position of the beam shown in Figs. 7a and 7b. For the case of PLIF90 the equation describing this line is:

$$\tan^{-1}\left(\frac{\sqrt{d(2(R-h)-d)}}{R-h-d}\right) = \frac{\pi}{4} - \frac{1}{2}\tan^{-1}\left(\frac{\sqrt{d(2(R-h)-d)}}{h+d}\right) \quad (1)$$

Equation 1 was solved numerically to obtain a value of  $d$  for a given  $h$ . The overestimation of the film thickness in raw PLIF,  $h_{app}/h_{real}$ , is then given by the term  $(h+d)/h$ . This quantity is plotted as a function of  $h$  in Fig. 7c by crosses. The solid red line on the same figure shows the analytical approximation proposed in Ref.[8] (see Eq. (4) in that paper). For PLIF with an angle  $\theta$  between the camera and the normal to the laser sheet plane, the situation is slightly different (see Fig. 7b). In this case Equation (1) is modified as:

$$\tan^{-1}\left(\frac{\sqrt{d(2(R-h)-d)}}{R-h-d}\right) = \frac{\pi}{4} - \frac{1}{2}\tan^{-1}\left(\frac{\sqrt{d(2(R-h)-d)}}{h+d}\right) - \frac{\theta}{2} \quad (2)$$

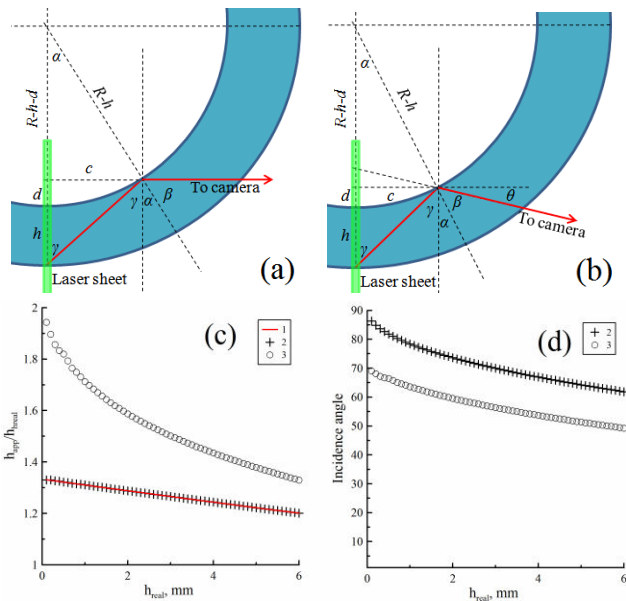


**Figure 7** Position of the false interface in raw PLIF: (a) at a right angle, and (b) at an angle  $\theta$ . (c) Overestimation of the film thickness in raw PLIF depending on film thickness: (1) analytical approximation in Ref. [8]; (2) PLIF90; (3) PLIF70 ( $\theta=20^\circ$ ). (d) Incidence angle for PLIF90 (2) and PLIF70 (3).

The value  $h_{app}/h_{real}$  is then given as  $(h + d + \sqrt{d(2(R-h)-d)}\tan(\theta))/h$ . This quantity for the case of PLIF70 ( $\theta=20^\circ$ ) is plotted by circles in Fig. 7c. In this case the overestimation of the true film thickness is indeed greater than in case of PLIF90. Figure 7d shows the values of incidence angle,  $\alpha+\gamma$ , for different film thicknesses. For both PLIF70 and PLIF90 this angle is always larger than the angle of TIR. Calculations show that this angle will eventually become lower than the critical angle with increasing  $\theta$ .

### Effect of transverse curvature on PLIF

It was mentioned above that sometimes a raw PLIF image (especially PLIF90) shows lower values of film thickness at the front slope of a wave compared to BBLIF. This effect may be related to the transverse curvature of the film. The idea in the case of PLIF is illustrated in Fig. 8a. If a wave is three-dimensional with negative transverse curvature, only the illuminated section of the pipe between the wall and Line 2 will be visible in the PLIF90 image. The part above Line 2 will not pass to the camera because of total internal reflection at the liquid-gas interface, e.g., Line 1. A three-dimensional shape with negative transverse curvature is typical at the fronts of waves on falling films far from the inlet, see, e.g., Ref. [12], who describe "horse-shoe" and "streak" waves. An example of a streak wave is shown in Fig. 8b. Thus, this discrepancy is most probable at the fronts of waves.

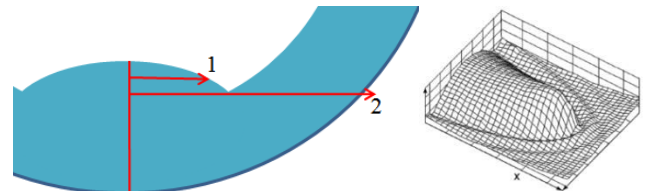


**Figure 8** (a) Sketch explaining how the PLIF technique would underestimate the film thickness when the transverse curvature of the film surface is negative. (b) Three-dimensional "streak wave" on a falling film, reproduction of Fig. 2b from Ref. [12].

An estimation of the transverse curvature was possible due to the scattering of the laser light, which made the whole film weakly illuminated. This light enables us to reconstruct the 3D-shape of the film surface, similarly to Ref. [10]. The film thickness data outside of the laser sheet are very noisy because of low illumination; nonetheless, it is possible to make a rough estimate of the film curvature in the transverse direction as a first coefficient in a parabolic approximation of a smoothed transverse profile,  $h(y)$ , over a width of 2.7 mm.

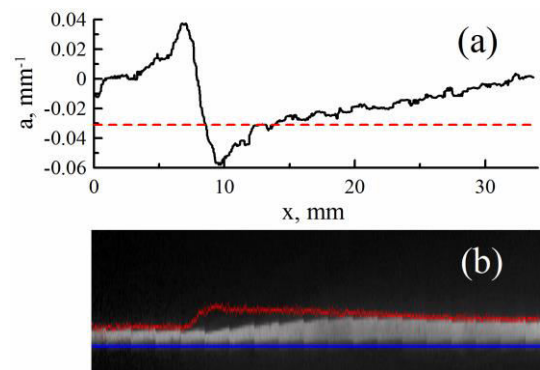


**Figure 9** (a) Variation of transverse curvature of the film along a wave's profile at  $Re_L=150$ ,  $V_g=0$ . Dashed red line shows the negative value of pipe curvature. (b) Raw PLIF90 image of the same wave. Blue line corresponds to the position of the wall; red dots show film thickness values measured with BBLIF.

Figure 9 shows:(a) an example of variation of transverse curvature with the longitudinal coordinate, together with (b)

superimposed PLIF90/BBLIF data on the same film profile. The raw PLIF90 signal is expected to underestimate the film thickness when the curvature is negative, while the BBLIF signal may be expected to overestimate it (Fig. 8a). It can be seen that the discrepancy between PLIF and BBLIF occurs in the area with largest negative transverse curvature of the film. This area corresponds to the front and the crest of the wave. It should be noted that a uniform film thickness actually corresponds to the positive curvature of the pipe, which is estimated in the same manner to be about  $0.031 \text{ mm}^{-1}$ . The case when the film surface is parallel to the axis of the PLIF camera is expected to occur when  $a$  is about  $-0.031 \text{ mm}^{-1}$  as shown by the red dashed line in Fig. 9(a).

Obviously, PLIF70 is less vulnerable to this kind of distortion, since the transverse slopes of the interfaces rarely reach large angles; thus, in the majority of cases, the top part of the illuminated section will be visible under such angle. Nonetheless, at the top of disturbance waves the fast ripples and especially liquid bags/ligaments may have higher transverse curvatures, leading to an underestimation of the film thickness by the PLIF method.

### Effect of steep slopes on BBLIF

One of the main shortcomings of the BBLIF technique is its vulnerability to an incident light intensity increase (focussing) and TIR of the laser light at steep slopes of the interface. Of these two the most significant is the latter. The local fluorescence brightness is directly proportional to the local illumination by the exciting light, which is contributed by both the passing beam and the beam reflected from the interface. At small interface slopes the reflection coefficient is typically small and the contribution of the reflected beam is also small and can be taken into account. At steep slopes, the contribution of the reflected beam is equal to that of the passing beam or even larger if the reflected light is locally focused by the curvilinear interface. Due to the nonlinear relation between the brightness of fluorescent light and film thickness, this may lead to extreme overestimation of local film thickness.

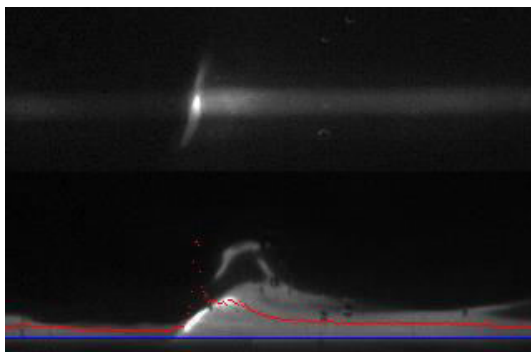


**Figure 10** Example BBLIF data distortion due to total internal reflection. Top: Raw BBLIF image with overbright area. Bottom: Raw PLIF70 image with BBLIF film thickness (red dots) and wall position (blue line).  $Re_L = 150$ ,  $V_g = 32 \text{ m/s}$ .

Such large angles are mostly observed at the front slopes of fast ripples on top of disturbance waves, which are of particular interest. They can also occur inside liquid bags or ligaments,

around the bubbles entrapped into the film and, rarely, at the fronts of slow ripples. An example of the latter event is shown in Fig. 10. In this frame a slow ripple wave with an unusually steep front is shown. The real shape of the front is assumed to correspond to the bright line in PLIF90, as mentioned previously. The top image shows that the overbright area is formed in a transversely oriented direction, corresponding to the position of the three-dimensional wave front. This bright line creates a narrow high-amplitude peak in the BBLIF data; the borders of this peak can be deduced from the local slope of the BBLIF interface. The problem is that not all the slopes are oriented in transverse direction. In order to account properly for such events, 3D measurements are highly recommended.

### Detection of bubbles

Another possible source of error typical when studying gas-sheared liquid films is related to presence of gas bubbles entrapped by liquid film. Ideally, the bubbles should be detectable but their presence should not obscure film thickness measurements. Figure 11a shows that the bubbles look like bright rings with dark centres in raw BBLIF images, which makes a bubble appear as a trough with high rim at the borders in film thickness records. This makes it possible to detect the bubble, measure its size, the thickness of film encompassing the bubble and to use this to estimate the thickness of the residual film (see Ref. [2]), although the result from this correction is non-trivial and is associated with some uncertainty.

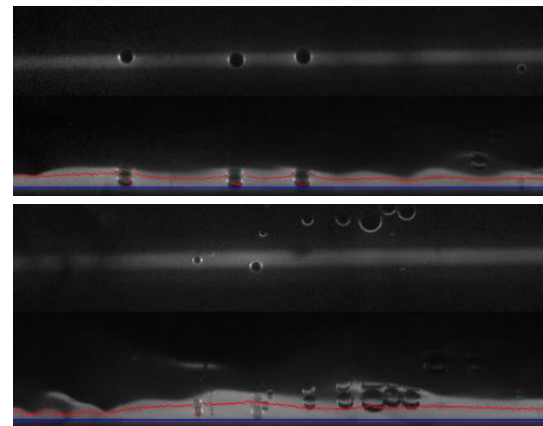


**Figure 11** Effect of bubbles on BBLIF signal (top); Appearance of out-of-plane bubbles in PLIF signal (bottom).

On the other hand, PLIF is also able to detect the bubbles and to measure their properties, especially when these are directly in the laser sheet whence the method is less susceptible to their presence. Nevertheless, an effort is still required to identify the true gas-liquid interface if multiple bubbles are present, and also, some ambiguities are possible as illustrated in Fig. 11(b). Here, bubbles located out of plane of the laser sheet are also visible in PLIF images if these are in the line-of-sight of the camera. Both ambiguities can be minimised: proper identification of the real position of the interface allows to eliminate the false bubbles and examination of the brightness distribution in the bubble image makes it possible to sort the bubbles into three groups: bubbles inside the laser sheet,

bubbles closer to the camera and bubbles farther from the camera. After such corrections, conventional PLIF can make a reliable method of studying bubbles. Alternative methods exist, for example, in using two cameras to eliminate non-common bubbles.

## CONCLUSIONS

Two methods of investigating interfacial gas-liquid flows, namely, brightness-based and planar LIF (also known as BBLIF and PLIF), were studied in detail. These are advanced highly detailed (spatiotemporally resolved) methods by comparison to the majority of other methods used for the measurement of these flows, which typically allow only pointwise data to be obtained and often distort the signal due to low spatial resolution. The two methods have their own challenges in application. A simultaneous application of both techniques was performed in order to identify these difficulties and to develop approaches by which to eliminate or minimise distortions of different types typical for each LIF approach. As a result, recommendations for the reliable employment of the BBLIF and PLIF methods are provided.

For the PLIF method, a decrease in the angle between the camera axis and the laser sheet from the traditional  $90^\circ$  is highly recommended. Though this will decrease the spatial resolution in the radial direction, it will minimise the underestimation of film thickness by the raw image when the interface is curved in the transverse direction, leading to simpler and smaller corrections to be applied when processing these raw images for the film thickness. A mirror effect, as predicted in Ref. [8], exists and yields a larger illuminated area in raw images than the liquid domain (true film thickness). However, the illumination field is different to that assumed in Ref. [8], in such a way that this can be compensated for by using the position of the bright line in the illumination field as the position of the true interface. Further investigation is being performed in relation to this point. A decrease in the PLIF angle to  $70^\circ$  increases the degree overestimation, but may lead to an elimination of the mirror effect at even smaller angles. When the film surface is highly agitated, the mirror effect becomes much weaker or disappears (see, e.g., Fig. 12).

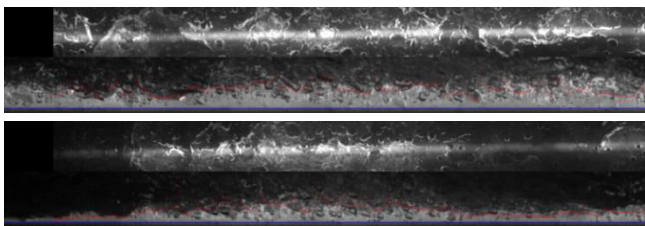


**Figure 12** Comparison of PLIF and BBLIF measurements in the disturbance wave regime, in which the mirror effect is much weaker. PLIF $70^\circ$ ,  $Re_L=1350$ ,  $V_g=39$  m/s.

It was confirmed that the BBLIF technique is vulnerable to high curvatures and total internal reflection at steep interface. These distortions may be compensated by identifying the areas with steep slopes and replacing the distortions with approximate shapes. For this reason, 3D measurements are

recommended when using the BBLIF method in order to avoid ambiguities with TIR distortions and bubbles.

Despite the issues listed above, each of the two methods are considered to be indispensable for the in-depth study of falling or gas-sheared liquid films, especially once the issues are accounted for. As an additional measure to enhance reliability, a simultaneous application of the two techniques can be used.

## ACKNOWLEDGEMENT

The work was supported by UK EPSRC Program Grant MEMPHIS (EP/K003976/1) and British Council "Researcher Links" programme (application 165900030).

## REFERENCES

- [1] Alekseenko, S.V., Antipin, V.A., Cherdantsev, A.V., Kharlamov, S.M., Markovich, D.M., Two-wave structure of liquid film and waves interrelation in annular gas-liquid flow with and without entrainment, *Physics of Fluids*, Vol. 21, 2009, pp.061701–061704.
- [2] Hann, D.B., Cherdantsev, A.V., Azzopardi, B.J., Study of bubbles entrapped into a gas-sheared liquid film, *International Journal of Multiphase Flow*, 2016 (submitted)
- [3] Hewitt, G.F., Jayanti, S., Hope, C.B., Structure of thin liquid films in gas-liquid horizontal flow, *International Journal of Multiphase Flow*, Vol. 16, 1990, pp. 951–957.
- [4] Schubring, D., Ashwood, A.C., Shedd, T.B., Hurlburt, E.T., Planar laser-induced fluorescence (PLIF) measurements of liquid film thickness in annular flow. Part I: Methods and data, *International Journal of Multiphase Flow*, Vol. 36, 2010, pp. 815–824.
- [5] Farias, P.S.C., Martins, F.J.W.A., Sampaio, L.E.B., Serfaty, R., Azevedo, L.F.A., Liquid film characterization in horizontal, annular, two-phase, gas-liquid flow using time-resolved laser-induced fluorescence, *Experiments in Fluids*, Vol. 52, 2012, pp. 633–645.
- [6] Zadrazil, I., Matar, O.K., Markides, C.N., An experimental characterization of downwards gas-liquid annular flow by laser-induced fluorescence: flow regimes and film statistics, *International Journal of Multiphase Flow*, Vol. 60, 2014, pp. 87–102.
- [7] Zadrazil, I., Markides, C.N., An experimental characterization of liquid films in downwards co-current gas-liquid annular flow by particle image and tracking velocimetry, *International Journal of Multiphase Flow*, Vol. 67, 2014, pp. 42–53.
- [8] Häber T., Gebretsadik M., Bockhorn H., Zarzalis N., The effect of total reflection in PLIF imaging of annular thin films, *International Journal of Multiphase Flow*, Vol. 76, 2015, pp. 64–72
- [9] Alekseenko, S.V., Cherdantsev, A.V., Cherdantsev, M.V., Isaenkov, S.V., Markovich, D.M., Study of formation and development of disturbance waves in annular gas-liquid flow, *International Journal of Multiphase Flow*, Vol. 77, 2015, pp. 65–75
- [10] Cherdantsev, A.V., Hann, D.B., Azzopardi, B.J., Study of gas-sheared liquid film in horizontal rectangular duct using high-speed LIF technique: three-dimensional wavy structure and its relation to liquid entrainment, *International Journal of Multiphase Flow*, Vol. 67, 2014, pp. 52–64.
- [11] Webb, D.R., Hewitt, G.F., Downwards co-current annular flow, *International Journal of Multiphase Flow*, Vol.2, 1975, pp. 35–49.
- [12] Kharlamov, S.M., Guzanov, V.V., Bobylev, A.V., Alekseenko, S.V., Markovich, D.M., The transition from two-dimensional to three-dimensional waves in falling liquid films: Wave patterns and transverse redistribution of local flow rates, *Physics of Fluids*, Vol. 27, 2015, pp. 114106